Arbitrary Bending Plasmonic Light Waves

Itai Epstein and Ady Arie*
Department of Physical Electronics, Fleischman Faculty of Engineering, Tel Aviv University, Tel Aviv 69978, Israel
(Received 24 October 2013; published 15 January 2014)

We demonstrate the generation of self-accelerating surface plasmon beams along arbitrary caustic curvatures. These plasmonic beams are excited by free-space beams through a two-dimensional binary plasmonic phase mask, which provides the missing momentum between the two beams in the direction of propagation and sets the required phase for the plasmonic beam in the transverse direction. We examine the cases of paraxial and nonparaxial curvatures and show that this highly versatile scheme can be designed to produce arbitrary plasmonic self-accelerating beams. Several different plasmonic beams, which accelerate along polynomial and exponential trajectories, are demonstrated both numerically and experimentally, with a direct measurement of the plasmonic light intensity using a near-field scanning optical microscope.

DOI: 10.1103/PhysRevLett.112.023903 PACS numbers: 42.25.-p, 73.20.Mf

Surface-plasmon polaritons (SPPs) are surface electromagnetic waves that are coupled to electron waves, which propagate at the interface between a dielectric and a metallic medium [1]. The ability to control and guide plasmonic light waves opens exciting new possibilities in photonics and electronics [2,3]. Specifically, nanoscale on-chip technologies such as surface plasmon circuitry [4], subwavelength optical devices [5,6] and nanoscale electro-optics [7], as well as new applications in biology and chemistry such as biosensing, optical trapping, and micromanipulation at the nanoscale [8], have attracted great interest in recent years.

In the last several years, new types of plasmonic beams have been realized that have unique properties. These beams can be "nonspreading" (i.e., preserve their spatial shape with propagation) as well as "self-accelerating" (i.e., propagate along curved trajectories). For example, the plasmonic Cosine-Gauss beam [9] is a nonspreading beam that propagates along a straight trajectory, whereas the plasmonic Airy beam [10–13] is nonspreading and propagates along a parabolic trajectory. The latter is so far the only self-accelerating plasmonic beam that has been demonstrated, and it is restricted to a parabolic trajectory. In this Letter, we address the question of whether it is possible to create self-accelerating surface plasmon beams that propagate along arbitrary curved trajectories.

The Airy function is an exact solution of the paraxial Helmholtz equation or, equivalently, of the Schrödinger equation for a free particle [14] that carries infinite energy. An actual Airy beam, however, carries finite energy and is obtained by truncating the infinitely long tail of the Airy function by using an exponential or Gaussian window [15]. The truncated Airy beam preserves its shape and self-accelerates, but only over a finite distance. Recently it was shown [16,17] that free-space nonspreading beams, propagating along arbitrary convex trajectories over finite distances, can be realized. However, the question still remains as to whether this concept, demonstrated so far only with free-space beams, can be used for the case of surface plasmon waves. If so, several fundamental challenges, owing to the plasmonic nature of the waves, should be addressed.

First, coupling a surface plasmon wave from a free-space wave requires a compensation for the missing momentum between the two wave vectors, as the plasmonic wave vector k_{SPP} is always greater than that of the free-space wave k_0 [18]. Second, owing to the limited propagation length of surface plasmons and the limited measurement range of characterization tools such as near-field scanning optical microscopes (NSOM), a significant acceleration is required over a fairly short propagation distance (typically $< 100\ \mu$m), meaning that the paraxial approximation would not be valid. Third, while planar phase plates readily provide a well-defined phase pattern for a free-space beam at the entrance plane, the surface plasmon is excited over a finite propagation distance, and therefore, its phase cannot be simply defined at a specific one-dimensional plane. Fourth and last, dynamic tools for controlling the wave front of free-space beams, like spatial light modulators (SLM), do not exist for surface plasmons. Despite these fundamental and practical challenges, we demonstrate here a robust method to excite self-accelerating surface plasmons propagating along arbitrary caustic trajectories. Specifically, we generate surface plasmons that propagate along several different polynomial and exponential trajectories.

To address the obstacles mentioned above, we introduce a two-dimensional binary plasmonic phase mask, which is analytically described by the following equation:

$$t(z,y) = \frac{h_0}{2}\left\{1 + \mathrm{sgn}\left[\cos\left(\frac{2\pi}{\Lambda}z + \phi_i(y)\right)\right]\right\}. \quad (1)$$

The mask is modulated periodically in the direction of propagation z with period Λ, and the resulting grating can

compensate for the missing momentum mentioned above. Furthermore, in order to excite a SPP that will follow a caustic trajectory, the desired initial phase $\phi_i(y) \equiv \phi(y, z = 0)$ is encoded in the transverse direction y. We emphasize that in contrast to planar phase plates for free-space beams, which operate only in the transverse direction, this binary plasmonic phase mask operates both in the propagation direction and in the transverse direction.

It is now required to derive the initial phase $\phi_i(y)$ corresponding to the desired analytical curve $y = f(z)$. The derivation is based on the principle that the caustic curve $f(z)$ can be constructed by multiple geometrical rays, which are tangent to the curve itself [17]. In our case, the transverse modulation of the phase generates these geometrical rays at angles $\theta(y)$ with respect to the z axis, where $d\phi_i(y)/dy = k \times \sin[\theta(y)]$ [17]. This sets the relation between the angle $\theta(y)$ and the caustic trajectory $f(z)$ to be

$$\frac{d\phi_i(y)}{dy} = \frac{kf'(z)}{\sqrt{1 + [f'(z)]^2}}, \tag{2}$$

where $f'(z) = df(z)/dz$. Under the paraxial approximation, this relation can be further simplified [16], thereby enabling one to obtain analytic expressions for the transverse phase of various trajectories. While this relation is utilized to obtain the one-dimensional initial phase $\phi_i(y)$ for the case of free-space waves, the generated plasmonic phase mask is two dimensional for the case of SPPs. To better understand how Eq. (2) and the geometrical rays principle relate to the plasmonic phase mask and the generated plasmonic beam, we offer a graphical representation of the construction of a caustic SPP, for the case of an exponential trajectory, in Fig. 1(c). This representation is the plasmonic equivalent of the representation for free-space waves demonstrated by [17]. It can be seen in Fig. 1(c) that the plasmonic phase mask generates geometrical rays at different angles, which are tangent to the constructed caustic SPP curve. The full discussion on exponential trajectory caustic SPP is presented later in the text.

First we examine the case of trajectories under the paraxial approximation and follow the procedure given by [16] to derive the phase for the following curves: $y = a_1 z^{1.5}$, $y = a_2 z^2$, $y = a_3 z^3$, and $y = b_1$, $\exp(q_1 z)$, where $a_1 = 34.1494 \times 10^{-3}$, $a_2 = 2.4691 \times 10^{-3}$, $a_3 = 2.7435 \times 10^{-5}$, $b_1 = 5 \times 10^{-7}$, $q_1 = 40 \times 10^{-3}$ are arbitrarily chosen constants (in micrometer units). For example, for the trajectory of $y = a_1 z^{1.5}$ the required transverse phase is $\phi_i(y) = \frac{9}{4}(a_1/2)^{2/3} y^{4/3}$.

The fabrication of the plasmonic phase masks was done by evaporating 200 nm of silver on a BK7 glass substrate, followed by electron-beam lithography of the mask pattern on PMMA (polymethyl methacrylate). A 50 nm silver layer was evaporated above the PMMA, followed by a lift-off process. The final device, shown in Fig. 1(a), consisted of a 50 nm thick binary plasmonic phase mask, on top of a

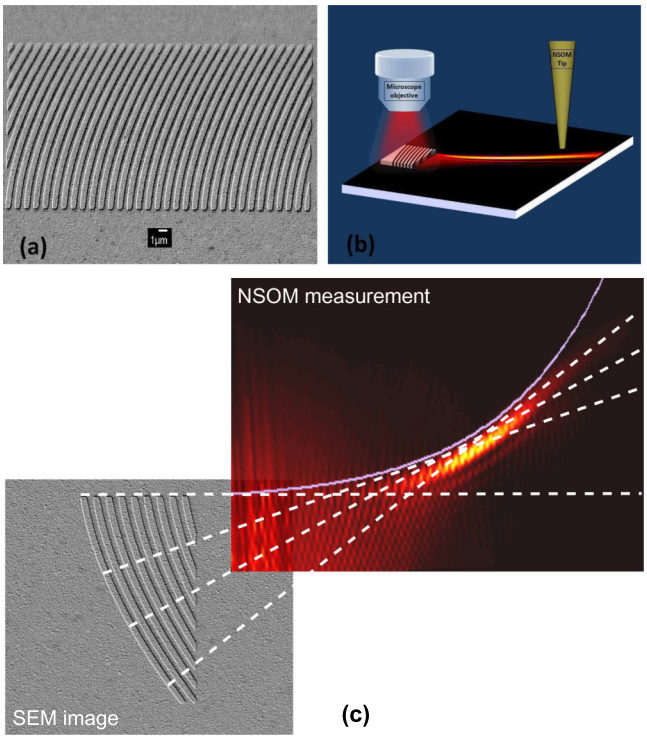

FIG. 1 (color online). (a) SEM image of the fabricated binary plasmonic phase mask for the case $y = a_1 z^{1.5}$. (b) Experimental setup. (c) Geometrical representation of the construction of a caustic SPP. Geometrical rays (white dashed lines) emanating from the two-dimensional plasmonic binary phase mask (SEM image) that generated the caustic SPP (NSOM measurement). The mask and the measured SPP are for the case of an exponential trajectory (the solid purple line shows the analytical curve).

200 nm layer of silver. The experimental setup, shown in Fig. 1(b), was composed of a fiber-coupled diode laser ($\lambda = 1.064$ μm), focused on the mask by a microscope objective lens, and a Nanonics MultiView 2000™ NSOM system that was used to measure the plasmonic light intensity. All the plasmonic phase masks were designed for free-space illumination at normal incidence, at which the surface plasmon wavelength is equal to the period of modulation Λ and the $m = 1$ order of the grating satisfies Eq. (2).

To simulate the intensity distribution of the generated plasmon waves, we realized a numerical calculation based on the two-dimensional Green's function of the Helmholtz equation. The experimental results and the numerical simulations for the different curves, under the paraxial approximation, are presented in Fig. 2, and it is clearly seen that the experimental results are in good agreement with the simulations. We note, however, that both numerical simulations and experimental results exhibit diffraction and deviation from the target analytical curve, depicted by the purple solid curve, in all of the examined trajectories. We believe that this is a manifestation of the paraxial approximation used to derive $\phi_i(y)$. In our experiment, all curves

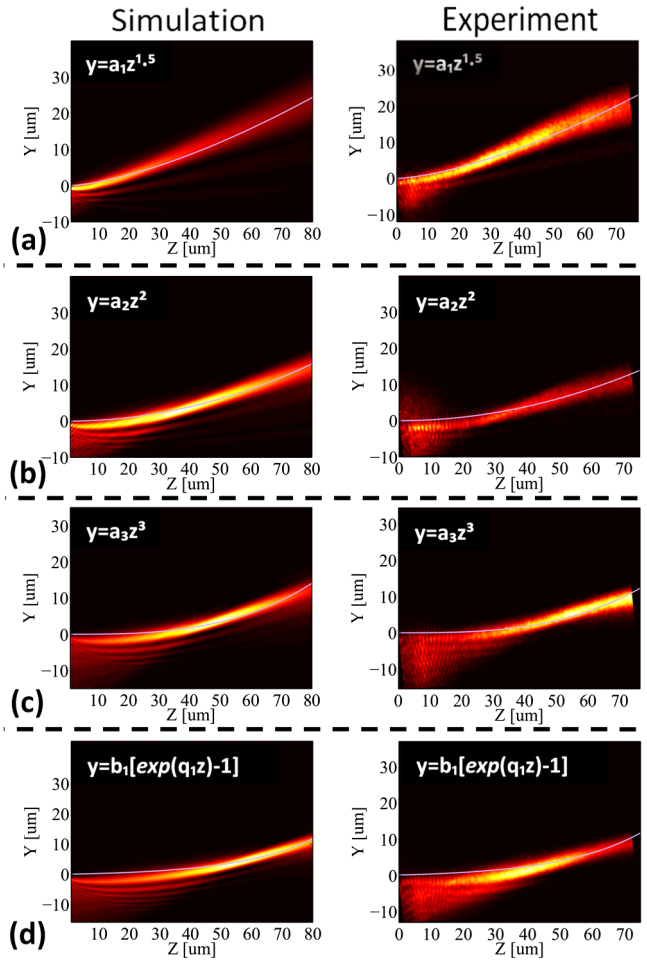

FIG. 2 (color online). Numerical simulations and experimental results for the following analytical curves derived under the paraxial approximation: (a) $y = a_1 z^{1.5}$, (b) $y = a_2 z^2$, (c) $y = a_3 z^3$, and (d) $y = b_1 \exp(q_1 z)$. The purple solid curves in all figures depict the target analytical curve $y = f(z)$.

were designed to exhibit the desired acceleration within 80 μm, corresponding to the scanning range limit of the NSOM system. This rapid acceleration is actually already beyond the paraxial limit, making this method applicable only to weaker accelerations, spanned on larger length scales. We also note that all figures were rotated between 3° and 5° as to align the coordinates of the target analytical curves with those of the scanning NSOM system. We relate the periodic intensity variations, transverse to the direction of propagation, appearing in the experimental results within the individual beam lobes, to interference between the plasmonic beam and the back-reflected free-space beam recorded by the NSOM; thus, they depend on the phase of the plasmonic beam [19].

We therefore examined the nonparaxial case next by following the procedure given by [17] to derive $\phi_i(y)$ using Eq. (3), for the same analytical curves. In this case Eq. (3) can be solved numerically in order to derive $\phi_i(y)$. Both the numerical simulations and the experimental results for the nonparaxial case are presented in Fig. 3. Once again, the agreement between the simulations and the measurements is clearly seen, but this time the beam closely follows the target analytical curve $y = f(z)$. The small deviations of the beam from the curve towards the end of the scan range are attributed to the Gaussian shaped illumination of the free-space beam, which results in a lower amplitude at the edges, and can therefore be reduced by uniformly illuminating the mask. Figures 3(d) and 3(e) show the results for two exponential trajectories, each with different constants, and both trajectories are shown in both figures for

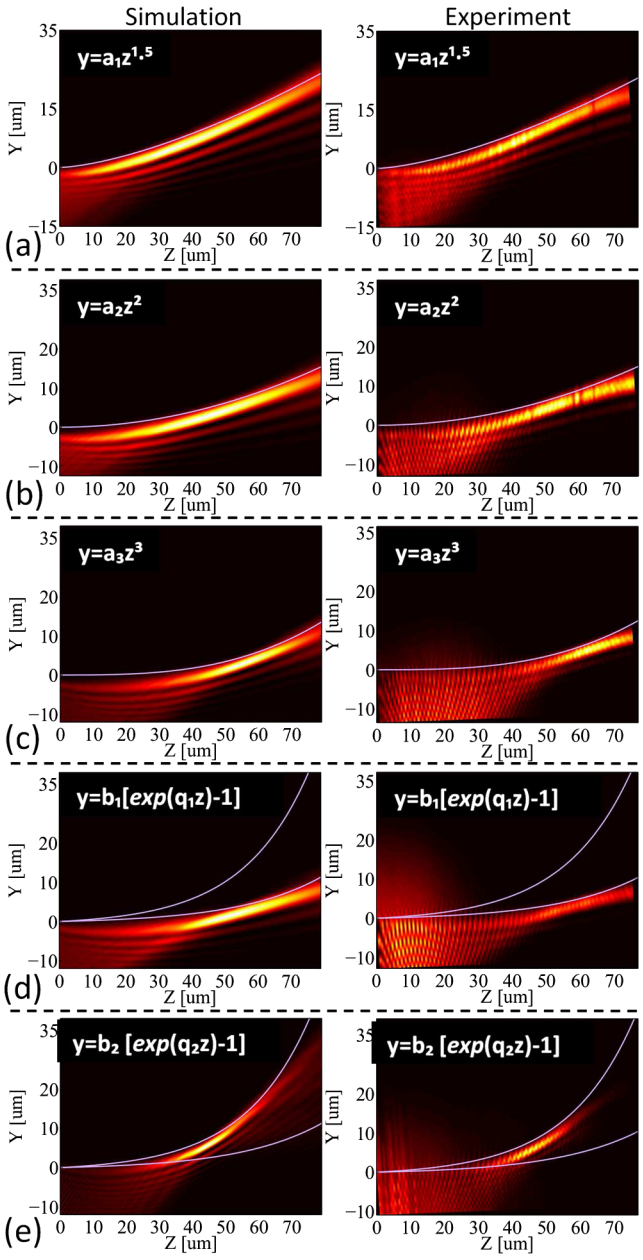

FIG. 3 (color online). (a)–(e) numerical simulations and experimental results for the same analytical curves presented in Fig. 2, only this time derived for nonparaxial curvatures.

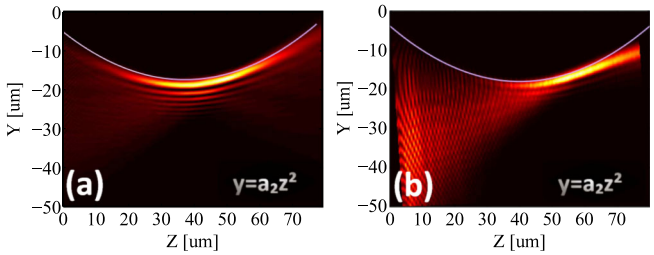

FIG. 4 (color online). (a) Numerical simulations and (b) experimental results of a nonmonotonic parabolic accelerating plasmonic beam.

comparison. In some of the measurements, a round halo surrounding the plasmonic beam can be observed owing to back-reflections of the free-space beam.

We can therefore conclude that for rapid accelerations on such short distances the nonparaxial method is indeed more suitable. Furthermore, this method is not limited only to monotonically increasing caustic curves. In order to illustrate the flexibility of the method, we show in Figs. 4(a) and 4(b) (simulation and measurement, respectively) a parabolic trajectory, but the initial transverse phase is set at a plane that is 40 μm to the left of the parabola's vertex. The trajectory therefore bends downwards at first and then, after the vertex point, rises upwards (see [18] for the mask image). This concept can be further extended to generate two mirror-imaged trajectories recombined after a certain distance [18]. This would be a two-dimensional "area-caustic" or "area-bottle" beam version of the "volume-caustic" beam demonstrated by [17], or the optical bottle-beam demonstrated by [20] in free space, and may enable us to trap particles to the dark area confined by the caustic curves [8].

Next we analyze the design considerations of the optimal plasmonic phase mask, with the main design parameter being the number of periodic cycles within the mask. For an ideal phase-only mask, the field emanating from the mask should have a uniform amplitude and the required one-dimensional phase $\phi_i(y)$. While this is easily obtained for free-space beams, reflected from a planar phase mask or SLM, in the case of the plasmonic phase mask this ideal state can be realized by applying the mask with a single cycle. Figure 5(a) shows simulations of the resulting amplitude and accumulated phase emanating from the single-cycle mask, for the case of a $y = a_2 z^2$. Unfortunately, coupling SPPs via a single-cycle grating is not an efficient process, and it results in a weak SPP intensity. However, adding additional periodic cycles to the mask results in two different effects—increasing the coupling efficiency on one hand, but changing the resulting amplitude and phase from their target values on the other hand. These effects are presented in Fig. 5(c) for a mask with nine periodic cycles. It can be seen that the amplitude is not uniform anymore and the accumulated phase exhibits a small increase at larger y values. The change in the

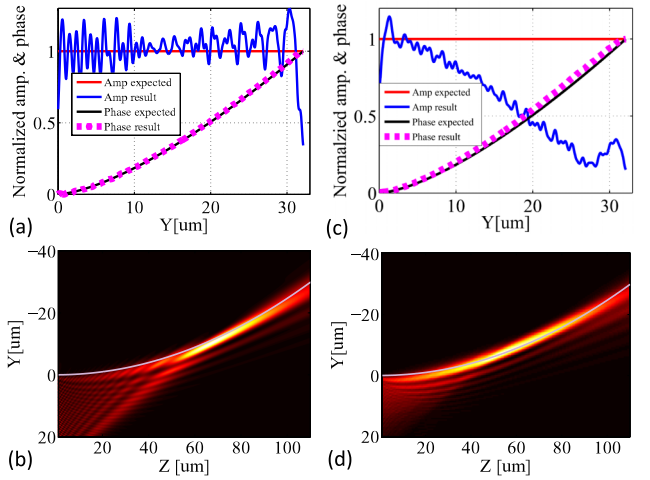

FIG. 5 (color online). Expected and resulting amplitude (red and blue curves, respectively) and accumulated phase (black and purple dashed curves, respectively) emanating from (a) a single-cycle mask and (c) a nine-cycle mask, for a $y = a_2 z^2$ curve. We show plasmonic beam intensity emanating from (b) single-cycle and (d) nine-cycle masks.

accumulated phase leads to a deviation from the target analytical curve, and the change in amplitude yields a change in the intensity distribution of the beam. These results are presented in Figs. 5(b) and 5(d).

In order to understand the origin of these effects, let us examine Eq. (1). The underlying assumption of that equation is that the propagation direction z and transverse direction y can be separated. However, since the plasmonic beam is accelerating, the transverse modulation also has an effect on the propagation axis. This is manifested in the fact that the thickness of the mask's grooves in the y direction at the bottom of the mask is smaller than those at the top [18]. This means that the light density coupled at that area is smaller, thereby leading to the unwanted variation in the amplitude of the generated surface plasmon. To resolve this issue we have considered a transformation of coordinates coinciding with those of the accelerating surface plasmon frame $\tilde{y} = y + f(z)$. This, however, yielded only a small improvement. We therefore found that the optimal solution is to limit the number of periodic cycles together with the transformation coordinates, and this solution was already implemented in the masks that generated the results for the nonparaxial beams [18]. We do emphasize, however, that implementing a single-cycle plasmonic phase mask can circumvent these problems at the cost of reduced coupling efficiency.

To conclude, we have demonstrated numerically and experimentally the generation of self-accelerating plasmonic light beams that propagate along arbitrary caustic trajectories. We examined the cases of paraxial and nonparaxial caustics and found the latter to be more suitable for the case of rapidly accelerating plasmonic light beams. We discussed the design limitations of the plasmonic phase

mask and found the crucial parameter to be the number of periodic cycles used in the mask. We believe that this demonstration of arbitrary self-accelerating surface plasmon waves will enable new exciting possibilities in photonics and electronics at the nanoscale. For example, these beams can enable the trapping and guiding of microparticles along the arbitrary curves, or they can allow one to circumvent an obstacle by designing a bypassing caustic. Moreover, we expect the method will be used for shaping the caustics of other types of waves, such as surface acoustic waves [21], ground radio waves, electron waves [22], etc.

The authors would like to acknowledge Dr. Yigal Lilach for the *e*-beam writing. This work was supported by the Israeli Science Foundation, Grant No. 1301/13.

*ady@eng.tau.ac.il

[1] S. Maier, *Plasmonics: Fundamentals and Applications* (Springer, New York, 2007).
[2] H. A. Atwater, Sci. Am. **296**, 56 (2007).
[3] M. L. Brongersma and V. M. Shalaev, Science **328**, 440 (2010).
[4] T. W. Ebbesen, C. Genet, and S. I. Bozhevolnyi, Phys. Today **61**, No. 5, 44 (2008).
[5] W. L. Barnes, A. Dereux, and T. W. Ebbesen, Nature (London) **424**, 824 (2003).
[6] D. K. Gramotnev and S. I. Bozhevolnyi, Nat. Photonics **4**, 83 (2010).
[7] E. Ozbay, Science **311**, 189 (2006).
[8] M. L. Juan, M. Righini, and R.Quidant, Nat. Photonics **5**, 349 (2011).
[9] J. Lin, J. Dellinger, P. Genevet, B. Cluzel, F. deFornel, and F. Capasso, Phys. Rev. Lett. **109**, 093904 (2012).
[10] A. Salandrino and D. N. Christodoulides, Opt. Lett. **35**, 2082 (2010).
[11] A. Minovich, A. E. Klein, N. Janunts, T. Pertsch, D. N. Neshev, and Y. S. Kivshar, Phys. Rev. Lett. **107**, 116802 (2011).
[12] P. Zhang, S. Wang, Y. Liu, X. Yin, C. Lu, Z. Chen, and X. Zhang, Opt. Lett. **36**, 3191 (2011).
[13] L. Li, T. Li, S. M. Wang, C. Zhang, and S. N. Zhu, Phys. Rev. Lett. **107**, 126804 (2011).
[14] M. V. Berry and N. L. Balazs, Am. J. Phys. **47**, 264 (1979).
[15] G. A. Siviloglou, J. Broky, A. Dogariu, and D. N. Christodoulides, Phys. Rev. Lett. **99**, 213901 (2007).
[16] E. Greenfield, M. Segev, W. Walasik, and O.Raz, Phys. Rev. Lett. **106**, 213902 (2011).
[17] L. Froehly, F. Courvoisier, A. Mathis, M. Jacquot, L. Furfaro, R. Giust, P. A. Lacourt, and J. M. Dudley, Opt. Express **19**, 16455 (2011).
[18] See Supplemental Material at http://link.aps.org/supplemental/10.1103/PhysRevLett.112.023903 for additional data and analysis.
[19] L. Yin, V. K. Vlasko-Vlasov, A. Rydh, J. Pearson, U. Welp, S. H. Chang, S. K. Gray, G. C. Schatz, D. B. Brown, and C. W. Kimball, Appl. Phys. Lett. **85**, 467 (2004).
[20] I. Chremmos, P. Zhang, J. Prakash, N. K. Efremidis, D. N. Christodoulides, and Z. Chen, Opt. Lett. **36**, 3675 (2011).
[21] A. J. Slobodnik, Proc. IEEE **64**, 581 (1976).
[22] N. Voloch-Bloch, Y. Lereah, Y. Lilach, A. Gover, and A. Arie, Nature (London) **494**, 331 (2013).